SEMIANNUAL STATUS REPORT

FOR PERIOD

SEPTEMBER 1, 1964, TO FEBRUARY 28, 1965

Required under the terms of NASA Research Grant nsG 376

"Theoretical and Experimental Studies
of the Underlying Processes and Techniques
of Low Pressure Measurement"

Under the direction of D. Alpert

By F. M. Propst

Coordinated Science Laboratory
University of Illinois
Urbana, Illinois

July, 1965

The areas of investigation included in the low pressure measurement studies have been changed somewhat during the past year. The program now includes studies of:

1. The pumping of getter-ion pumps at low pressures,
2. A crossed field mass spectrometer of high sensitivity and moderate resolution,
3. Secondary electron emission using high resolution,
4. The angular distributions of electrons and ions leaving a solid surface due to electron and ion impact,
5. The kinetics of gaseous adsorption and desorption.

It will be noted that several of the programs now included under this contract involve the study of surfaces and surface processes. During the past few years, it has become increasingly clear that a better understanding of such processes is required in many areas of ultrahigh vacuum technology.

The evaluation program for the suppressor ionization gauge has been completed. The results of this program are given in the attached report. Descriptions of the above programs are given below.

1. PUMPING OF GETTER-ION PUMPS AT LOW PRESSURES

1.1 Introduction

Getter-ion pumps have been used for about 10 years to obtain low pressures. Their operating principle is the following: A Penning discharge is maintained in a volume which is contained by a cylindrical or rectangular cell. The cell is maintained at 3000-6000 volts (anode, positive) and on each end is a plate at ground potential (cathode). A magnetic field perpendicular to the cathodes serves to increase the path length of electrons which oscillate back and forth between the cathodes. They ionize some of the gas molecules in the volume, and the latter are collected by the cathode.

Gas removal occurs in two different ways: The first is by ion pumping which can occur when ions enter the cathode metal with such an energy that they are trapped inside the crystal structure. The second way is gas removal by gettering. The cathode is made from a metal with good gettering characteristics (usually titanium). Ions impinging on the cathode sputter away some of the cathode material which serves as fresh gettering material. It is easy to see that these two methods compete.

It is well known that the pumping speed for getter-ion pumps is fairly constant over a pressure range from about 10^{-3} to 10^{-8} or 10^{-9} Torr. The pumping speed for noble gases (which are ion-pumped) is about an order of magnitude lower than for gases which are gettered. Below

a certain critical pressure p_c (which depends on different pump parameters) there is a rapid decrease in pumping speed.[1]

No results on the actual pumping speed, s, of getter-ion pumps below 10^{-9} Torr are published but only related parameters as discharge intensity,[1] I/p, or the rate of pressure arise after turning off the pump.[2,3]

Getter-ion pumps show a strong memory for gases which they have pumped, especially noble gases. No quantitative results on memory effects could be found in the literature.

1.2 Area of Investigation to Present

The goal of this experiment is to measure the actual pumping speed of a getter-ion pump to the lowest pressures obtainable and to compare it to the discharge intensity, I/p, and the ratio of gas flow to electric current,[4] ps/I. Furthermore, we wish to study the dependence of pumping speed on previously pumped gases. Experiments with pump models are being performed. These have a hot cathode electron

---

[1] Rutherford, S. L., "Sputter-Ion Pumps for Low Pressure Operation," Vac. Symp. Trans., 185-190 (1963).

[2] Klopfer, A., "Die Erzeugung von Hochstvakua Mit Getter-Ionenpumpen und Das Messen von Sehr Tiefen Drucken," Vakuumtechnik 10.4, 113-118 (1961).

[3] Davis, W. D., "Sputter-ion Pumping and Partial Pressure Measurements Below 10^{-11} Torr," Vac. Symp. Trans., 363-370 (1962).

[4] Jepsen, R. L., "Important Characteristics of a New Type Getter-Ion Pump," Le Vide, 80.80-89 (1959).

source which should enable them to maintain a reasonable pumping speed to lower pressures.

1.3 Experimental Method and Apparatus

We use the two gauge method after Landfors and Hablanian.[5] The pumping speed is calculated from the pressure drop along a known conductance between gas inlet and pump (see Fig. 1.1). The formulas are:

$$s_m = g_1 \cdot \frac{p_1 - p_2}{p_2 - p_0} \cong g_1 \cdot \left(\frac{p_1}{p_2} - 1\right) \quad \text{if } p_2 \gg p_0$$

$$\frac{1}{s} = \frac{1}{s_m} - \frac{1}{g_2} \quad , \text{ where}$$

s_m = measured pumping speed in liters/second at gauge 2

s = pumping speed of getter-ion pump taking into consideration conductance g_2

g_1 = calculated conductance between gauge 1 and gauge 2 in liters/second

g_2 = calculated conductance between gauge 2 and getter-ion pump

p_1, p_2 = measured pressures

p_0 = ultimate pressure of getter-ion pump.

---

[5] Landfors, L. A. and Hablanian, M. H., "Diffusion Pump Speed Measurements at Very Low Pressures," Vac. Symp. Trans., 363-370 (1962).

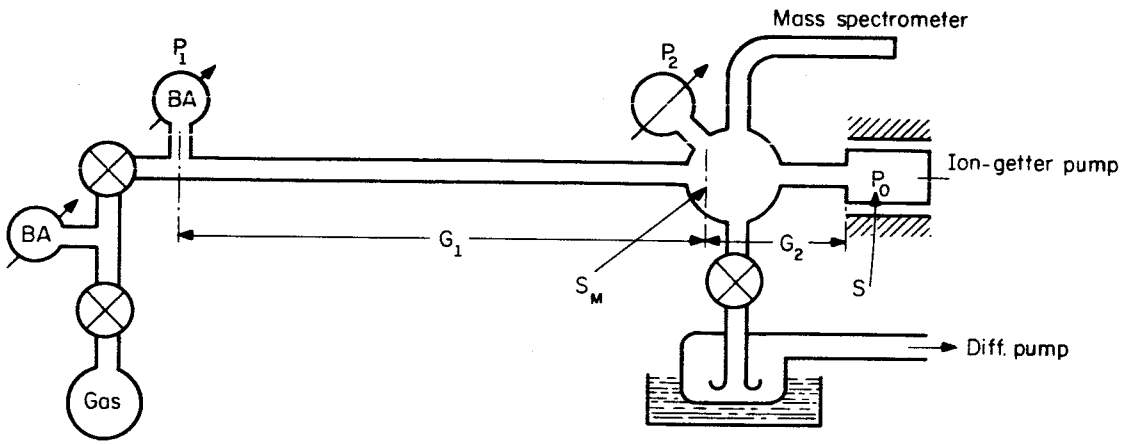

$$S_M = G_1 \frac{P_1 - P_2}{P_2 - P_0} \cong G_1 \left(\frac{P_1}{P_2} - 1 \right) \text{ if } P_2 \ll P_0$$

$$\frac{1}{S} = \frac{1}{S_M} - \frac{1}{G_2}$$

Fig. 1.1. Schematic View of Vacuum System Used for Pumping Speed Measurements.

BA: Bayard-Alpert ionization gauge

G_1, G_2: Conductances

P_0, P_1, P_2: Pressures at corresponding points

S_m, S: Measured and actual pumping speed

The vacuum system, with a volume of about two liters, was made of Pyrex glass (Corning 7740). Beginning at the high pressure side (gas inlet) it consisted of the following parts: Two all-metal valves (Granville-Phillips) were used in series to introduce gas from a one liter flask (Linde). A Bayard-Alpert gauge serves as an ion-pump to keep the pressure between the valves at 10^{-4} to 10^{-6} Torr. Without pumping, the pressure builds up to such values that the leak rate through the second valve is higher than desired even if both valves are closed completely. A Bayard-Alpert gauge measured the pressure at the beginning of the calculated conductance g_1, a Schuemann suppressor gauge[6] at its end. This end was connected to the getter-ion pump (15 liters/second VacIon pump by Varian), a partial pressure analyzer made by General Electric[7] and through a one-inch valve to an oil diffusion pump. Backstreaming oil was trapped with a zeolite trap[8] which could be cooled with liquid nitrogen.

The vacuum system was brought to low pressures in the following way: After glassblowing we baked the zeolite trap and the adjacent glass tubing for about three hours at 300°C with a valve between system and trap closed. Then the trap was cooled and immersed in

---

[6] Schuemann, W. C., "Ionization Vacuum Gauge with Photocurrent Suppression," Rev. Sci. Instr. 34.6, 700-702 (1963).

[7] David, W. D. and Vanderslice, T. A., "A Sensitive High-Speed Mass Spectrometer for Ultrahigh Vacuum Work," Vac. Symp. Trans., 417 (1960).

[8] Biondi, M. A., "High Speed Nonrefrigerated Isolation Traps for Ultrahigh Vacuum Systems," Rev. Sci. Instr. 30.831 (1959).

liquid nitrogen, and the valve opened and the system baked at 300°C for about half a day. Then the gauges were outgassed at 100 watts for 10 hours and the whole cycle repeated once more. One day after finishing the second outgassing, pressures around 1×10^{-11} Torr were regularly obtained. Lange[9] suggested this separation of trap and system during bakeout which gives pressures at least one order of magnitude lower than when trap and system are baked at the same time. Atmospheric helium diffusing through the glass walls was the main residual gas.

1.4 Results

1.4.1 Pumping Speed

We found it very difficult to define the practical meaning of pumping speed for getter-ion pumps. Literature studies and our own measurements showed clearly that it depends strongly on the previous life of the pump, especially on the type and amount of gas already pumped. It is impossible to talk about equilibrium conditions without defining them exactly, because when gas is pumped for an infinite time even at very low pressures, the pump will finally saturate, and the pumping speed will go to zero (see Fig. 1.2). Two different cases have been investigated:

a) Optimistic Case: The vacuum system was brought to the lowest pressure and the gas under consideration introduced beginning with very small influx. After waiting for about 10 minutes, data were taken and the pressure increased. The pumping speed did not increase

---

[9] Lange, W. J. To be published.

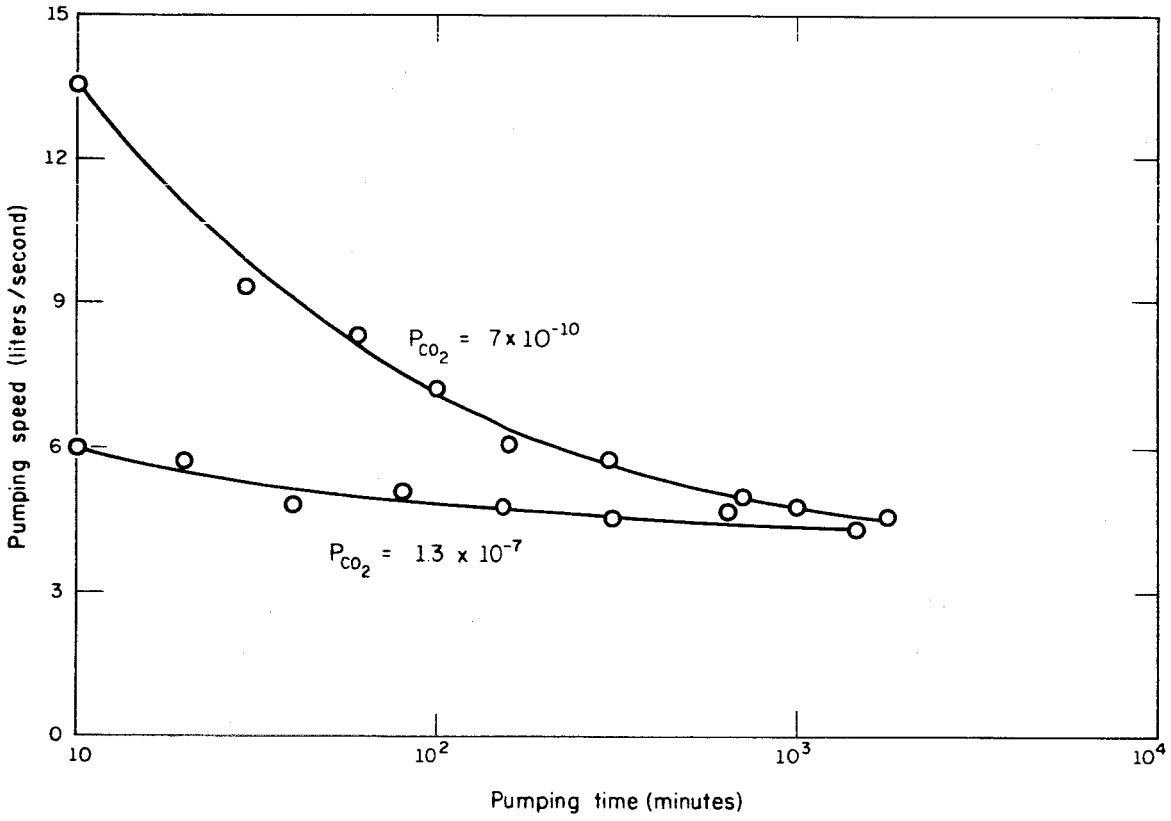

Fig. 1.2. Pumping Speed as a Function of Pumping Time of a Typical Getter-Ion Pump.

more than 20 per cent within 10 minutes after taking data; on the other hand, it did not reach a steady value even after hours.

b) Pessimistic Case: This time the pressure was decreased starting from about 10^{-6} Torr, and we waited about 30 minutes before taking data. Again the pumping speed did not change significantly when waiting much longer.

The curve for pumpdown of the volume only, without additional gas influx, must be somewhere between these curves. It has been found[10] that this type of pump is only capable of pumping down a system of a few liters to $2 - 5 \times 10^{-10}$ Torr.

We measured the pumping speed of a clean system without applying any voltage to the pump. Surprisingly high values (up to 5 liters/second) were found for a time which corresponds to the coverage time for one monolayer. Then it decreased continuously to zero. Further experiments with different gases and different pump treatments are planned. This result shows clearly that at least the low pressure part of our "optimistic" pumping speed results is strongly influenced by adsorption on clean surfaces of the pump, and up to 50 per cent of the measured speed can be accounted for by this process.

The most meaningful result for pumping speed is therefore a curve which gives the pumping speed as a function of time at constant pressure. Fig. 1.2 shows some results, and further measurements are being performed. The saturation of the pump is clearly visible.

---

[10] Rutherford, loc. cit.

Fig. 1.3 shows "optimistic" and "pessimistic" curves of pumping speed for helium and nitrogen. Measurements for other gases will follow soon. The "pessimistic" curve comes closer to the practical application where a system at forepump pressure has to be evacuated (from about 1×10^{-3} Torr). This curve shows that the onset of pumping action begins at different pressures for different gases. The critical pressure p_c, which has been defined in the introduction as the pressure below which the pumping speed decreases rapidly, depends also on the gas. For helium, the onset and the critical pressure is about two orders of magnitude higher than for nitrogen.

1.4.2 Pumping Speed vs. Discharge Intensity and ps/I

Table I gives some values for the ratio of gas flow to electric current. This ratio is constant for a single curve on Fig. 1.3 over the whole pressure range, but it differs from one gas to another and also from "optimistic" to "pessimistic" case. The discharge intensity I/p was found to be proportional to the pumping speed within the accuracy of our measurements ($\pm$ 10 per cent in general). To increase the pumping speed, it is necessary to increase the pump current, I, at a given pressure. The addition of electrons by means of a hot filament is a simple method.

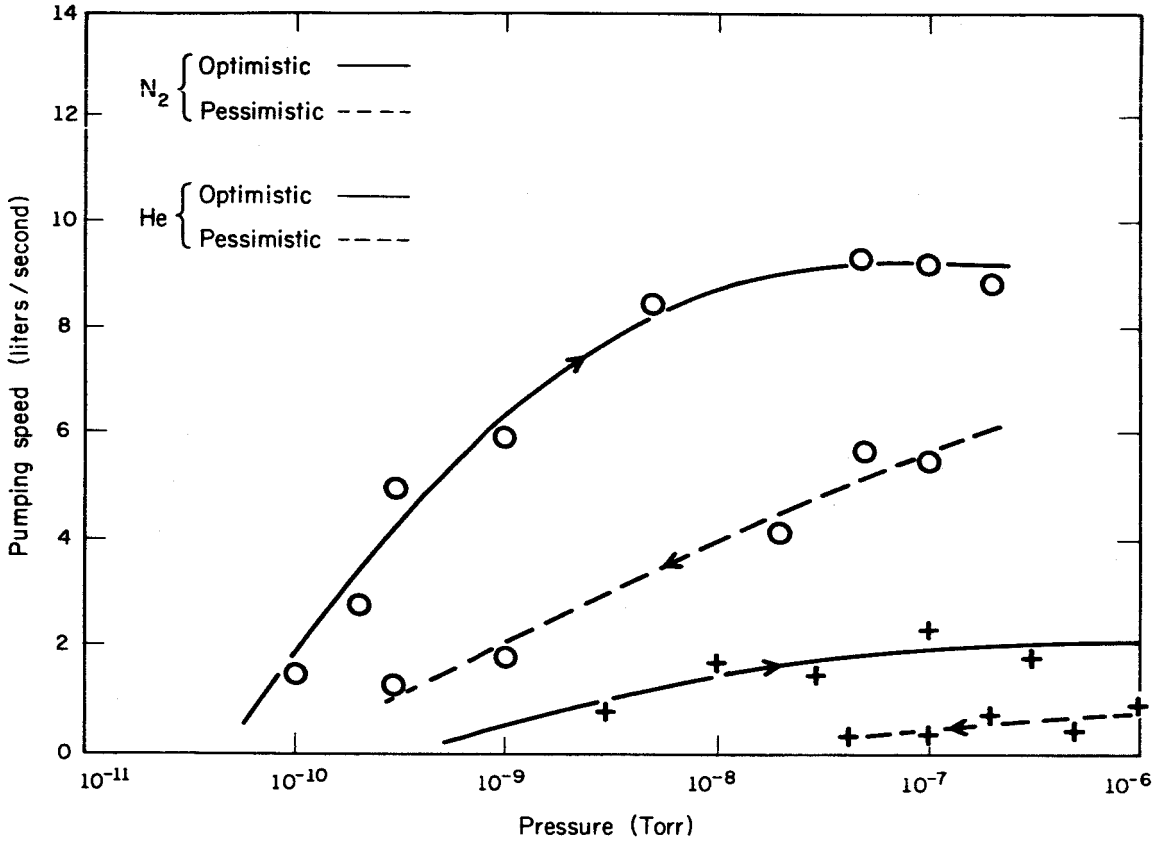

Fig. 1.3. Pumping Speed as a Function of Pressure of a Typical Getter-Ion Pump

Table I

Gas	Process	Investigated Pressures Lowest	Highest	ps/I in Molecules/charge
He	optimistic	1×10^{-9}	1×10^{-6}	0.6 ± 0.1
	pessimistic	5×10^{-9}	1×10^{-6}	0.3 ± 0.1
N_2	optimistic	1×10^{-10}	1×10^{-7}	0.9 ± 0.1
	pessimistic	3×10^{-10}	1×10^{-7}	0.5 ± 0.1

1.4.3 Memory Effects for Previously Pumped Gases

The saturation of a pump (see Fig. 1.2) is one type of memory effect which has been investigated. In another experiment we observed the memory effect in a pump which had pumped 10^{-2} Torr-liter of helium. After bakeout, the pump showed only a very small spontaneous emission rate. However, as soon as it started to pump nitrogen, the buried helium was resputtered, and the helium partial pressure was always proportional and of the same magnitude as that for nitrogen. The reverse effect could not be found; i.e., earlier pumped nitrogen was not resputtered by helium in an appreciable amount. This shows that helium is mainly ion-pumped, nitrogen not.

To erase the pump memory for helium, nitrogen was introduced to such a high pressure that the pump operated at an input of about 200 watts. Resputtering and strong heating reduced the amount of helium which was released under subsequent operation to a very small fraction compared to the gas which was pumped. The cleanup process could be followed very nicely with the partial pressure analyzer.

Further memory effect investigations are planned.

1.4.4 Pump Models with Hot Cathode Electron Source

There are strong indications that the decrease in pumping speed at lowest pressures is due to the lack of electrons which could ionize the few molecules left in the pump volume or, in other words, the path length of the electrons in the volume is too short before they hit the anode. By increasing the magnetic field or the anode cell diameter, Rutherford[11] could maintain high pumping speeds to pressures several orders of magnitude lower than usual. On the other hand, the introduction of additional electrons by a hot filament should have the same effect, and one could hope to maintain a reasonable pumping speed to even lower pressures than by changing the pump parameters only.

To check this hypothesis, pump models with a hot filament electron source were built. Fig. 1.4 shows such a model. The idea is taken from Lafferty[12] who built a hot cathode magnetron ion gauge of very similar structure for operation down to 1×10^{-14} Torr. Our earlier models had bad outgassing characteristics, and only pressures in the 10^{-9} region could be obtained. We changed to an anode made from platinum instead of titanium, and the filament support was changed too. No results have been found yet.

---

[11] loc. cit.

[12] Lafferty, J. M., "A Hot Cathode Magnetron Ionization Gauge for the Measurement of Ultra High Vacua," Vac. Symp. Trans., 97-103 (1960).

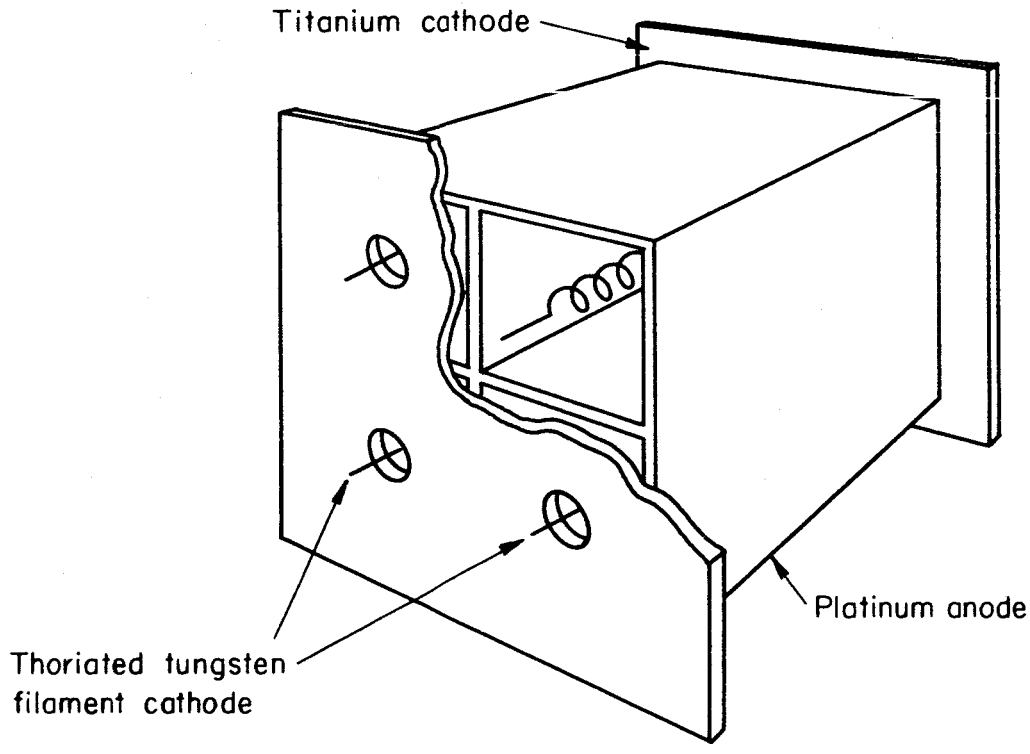

Fig. 1.4. Experimental Pump.

1.5 Conclusions

The pumping speed of a getter-ion pump decreases with time.

The most meaningful pumping speed curves are therefore those which give the pumping speed as a function of time at a given pressure.

To increase the pumping speed at a given pressure, the electric pump current has to be increased. A hot filament as an electron source is supposed to have this effect.

2. CROSSED FIELD MASS SPECTROMETER

During the last six months, an idea for a new type of mass spectrometer has been investigated. The theoretical performance has been calculated and the first experimental model built and operating. It is hoped that this mass spectrometer will have a sensitivity of 10^{-2} amps/Torr and a resolution of 25. It requires no more electronics than a Bayard-Alpert gauge and could read well into the ultrahigh vacuum region without an electron multiplier. The results of the tests which will be performed on this instrument will appear in the next report.

3. HIGH-RESOLUTION SECONDARY EMISSION

3.1 Introduction

Secondary emission has been the object of a great deal of study since its discovery around the turn of the century. Although of great practical importance, this work has not contributed greatly to our understanding of the solid state or surfaces. The primary reasons for this are:

a. The lack of control.

It was early recognized that secondary emission is strongly dependent on the condition of the surface; however, it has only been in the past few years that the techniques of ultrahigh vacuum and surface preparation have been developed to a degree sufficiently sophisticated to allow good control over surface experiments.

b. Poor resolution.

Typically, secondary experiments have consisted of a source of electrons (a hot filament), a means for focusing these onto a target, and some type of analyzer to determine the energy distribution of the ejected electrons. In such an arrangement, the best resolution that can be achieved is equal to the thermal spread of the incident beam ($\gtrsim$0.2 eV).

c. The lack of substantial theoretical support.

The difficulty of meaningful calculations on surface problems has in general made the field unattractive to

theoreticians. There has been some change in this attitude recently, however, and hopefully this positive trend will continue.

Many difficulties have been substantially eliminated during the past few years, and it seems that secondary emission can be a very useful tool for the study of a number of processes. Some of the possibilities will be discussed briefly.

The secondary electrons leaving a surface can be divided into two broad classes: the primary electrons scattered (elastically or inelastically) from the surface, and electrons excited from the surface due to the primaries. This classification is different from the normal "true secondary" and "elastic" division. The truly elastically scattered electrons constitute a small part of the total secondaries. This elastic process involves a transition in which the whole lattice takes up the momentum change in the collision, much in the same manner as in the Mössbauer effect. Grouped closely around these truly elastically scattered electrons (and with typical resolutions indistinguishable from the elastic content) are "almost" elastically scattered electrons, i.e., electrons that scatter with the emission or adsorption of a phonon (virtual or real). It should be possible, then, with a system of adequate resolution to study this second type of scattering in detail. In particular, it should be possible to study the excitation of the vibrational states of adsorbed gas specie on the surface.

In addition to vibrational states, the adsorbed atoms on surfaces have electronic transitions available for excitation. It is

felt that these transitions can also be detected by secondary emission studies.

The excitation of plasmons by electron impact has been observed by numerous experimenters. In general, the measurements have suffered from the lack of good control of the surface contamination. Again, an experiment under good control and with high resolution can yield much important information concerning the intensity of the plasmon excitation as a function of the primary energy, the width of the plasma excitation as a function of the primary energy, and the influence of surface coverage and surface damage.

Other processes which can give rise to discrete energy losses are the excitations of: a) optical defects, b) donor and acceptor levels in semiconductors, c) Tamm type surface states, and d) inner core states. The only type of all of the above processes which has been observed and identified is the plasmon excitation. We cannot say a priori which of the mechanisms will definitely be amenable for study by this technique; however, over the entire energy range available, it seems likely that most of them can at least be observed. In particular, if the energy loss spectra shows characteristic structure for adsorbed gas specie, we will have available a quantitative tool for the study of gas-surface reactions.

All of the above mechanisms would result in electrons emanating from the surface with characteristic energy losses below the primary energy (the first class of electrons). The second class of electrons would also be a valuable source of information concerning the interaction of electrons with electrons and with phonons.

This is a brief listing of the types of processes which we expect to observe and study. A brief description of the instrument constructed for this work follows.

3.2 Experimental Apparatus

A schematic of the apparatus constructed for high-resolution studies of secondary electron emission is shown in Fig. 3.1. Electrons pass from the electron source into the first energy analyzer (monochromator), the electrons from the monochromator strike the target and produce secondary electrons. Those secondaries leaving the target at the proper angle enter the second analyzer (analyzer), which determines the energy distribution of these electrons. An electron multiplier is used as the detector of the electrons leaving the analyzer, and either an electrometer or counting techniques can be used to monitor the output of the multiplier.

Fig. 3.2 is a more detailed drawing of the apparatus. With this drawing in mind, several design considerations will be discussed. Since we want to work to very low energies, it is necessary that considerable care be exercised to minimize the deleterious effects of magnetic fields and space charge. To illustrate, the radius of curvature of 1 eV electrons in a 500 milligauss field is about 6 centimeters, and an electron density of 10^6 electrons/cm^3 changes the potential from the vacuum value by 2.25 volts in one centimeter.

3.2.1 Magnetic Fields

Clearly, the earth's magnetic field must not enter the working region. A shield structure consisting of three concentric boxes

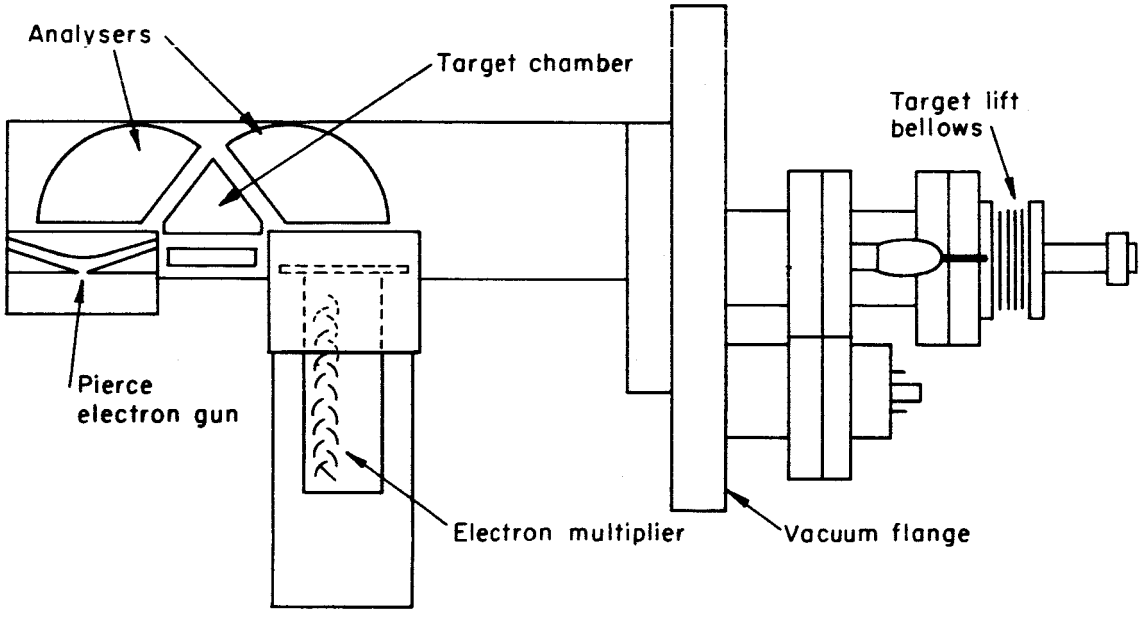

Fig. 3.1. Schematic of the Secondary Electron Experiment, showing the electron gun, the analyzers, and the electron multiplier arrangement.

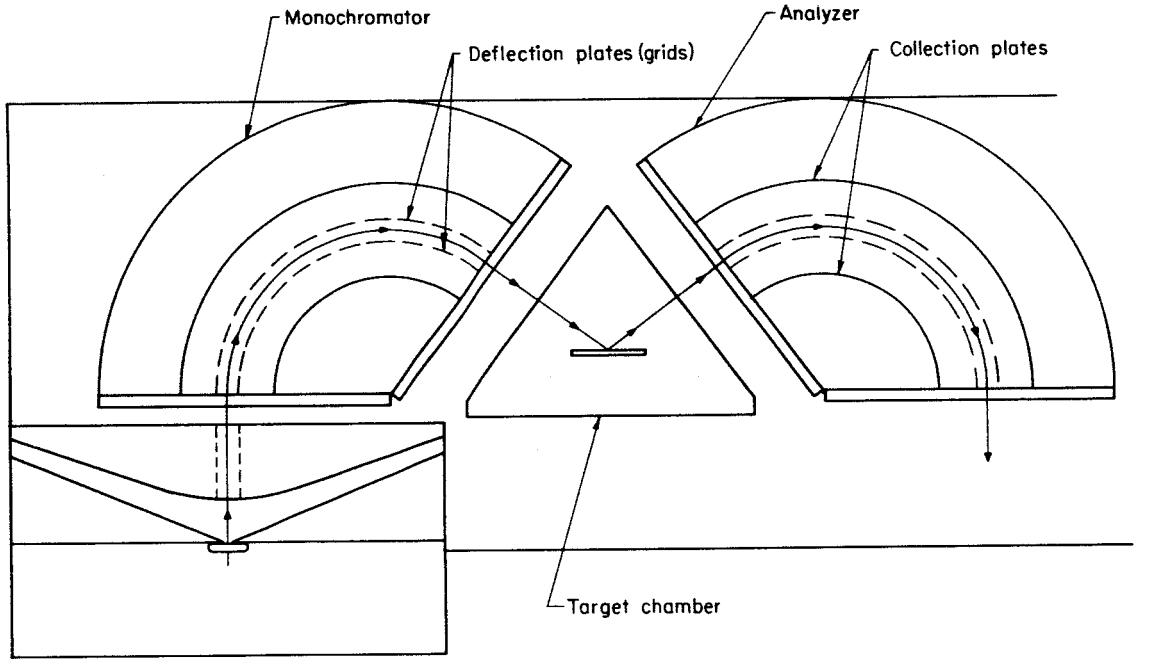

Fig. 3.2. Schematic of the Monochromator-Analyzer System, showing the deflection plate grids and the electron collection plates.

constructed of high permeability CoNetic AA material prevents this from happening. Calculations, based on the radii of curvature due to magnetic fields, show that the field in the apparatus must be less than a few milligauss for 1 volt electrons to pass through the apparatus without consequential perturbation. The cathode heating current gives rise to a magnetic field in an extremely critical region, since the energy of the electrons is very low near the cathode. Fig. 3.3 shows field versus distance for a single wire and a dipole wire each carrying 0.1 ampere. An indirectly heated cathode with a twelve-pole heater is used. The field from this heater drops off much more rapidly than that of the dipole.

3.2.2 Space Charge

We have taken several precautions to minimize the effects of space charge. First the electron source is a Pierce electron gun which matches potential between Laplace and Poisson regions so that the beam moves parallel to the axis of the gun. Use of a low temperature cathode produces electrons with a substantially narrower thermal energy distribution than high temperature cathodes. (The indirectly heated cathode also prevents IR drops and the associated energy spread.) Fig. 3.4 shows dI/dE for two cathodes, one with a work function three times the other. The curves are normalized so that dI/dE in both cases is the same in the region of the maximum, where the monochromator is tuned. The conclusions one can draw are: If $\varphi_1 = K\varphi_2$, T_1 must nearly equal KT_2 in order for $(dI/dE)_{1\ max} = (dI/dE)_{2\ max}$. If $T_1 = KT_2$, the total emitted current from cathode one is K times the total current from

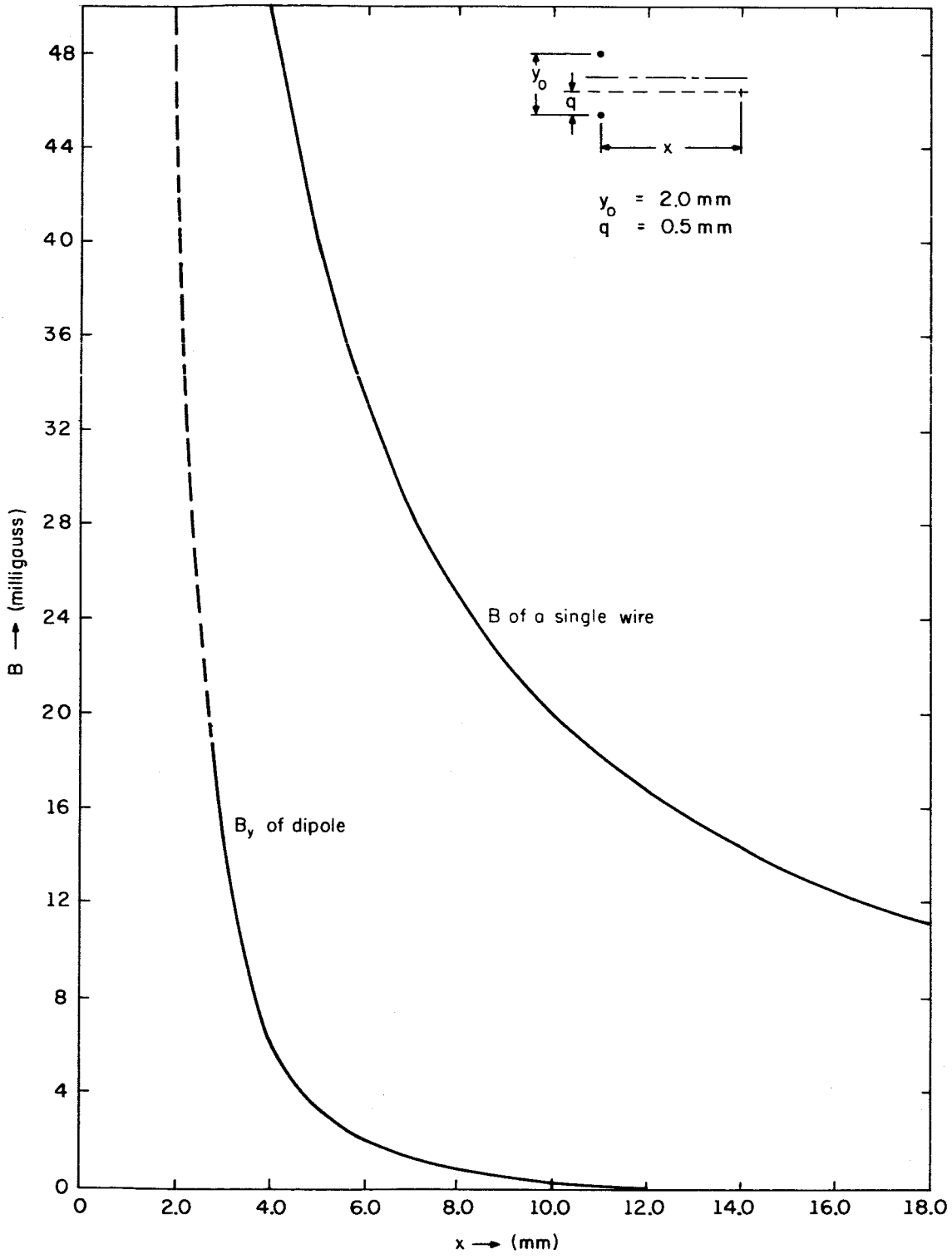

Fig. 3.3. Magnetic Field Produced by a Monopole and a Dipole as a Function of the Distance from the Axis of the Pole. The current is 0.1 amp in each case.

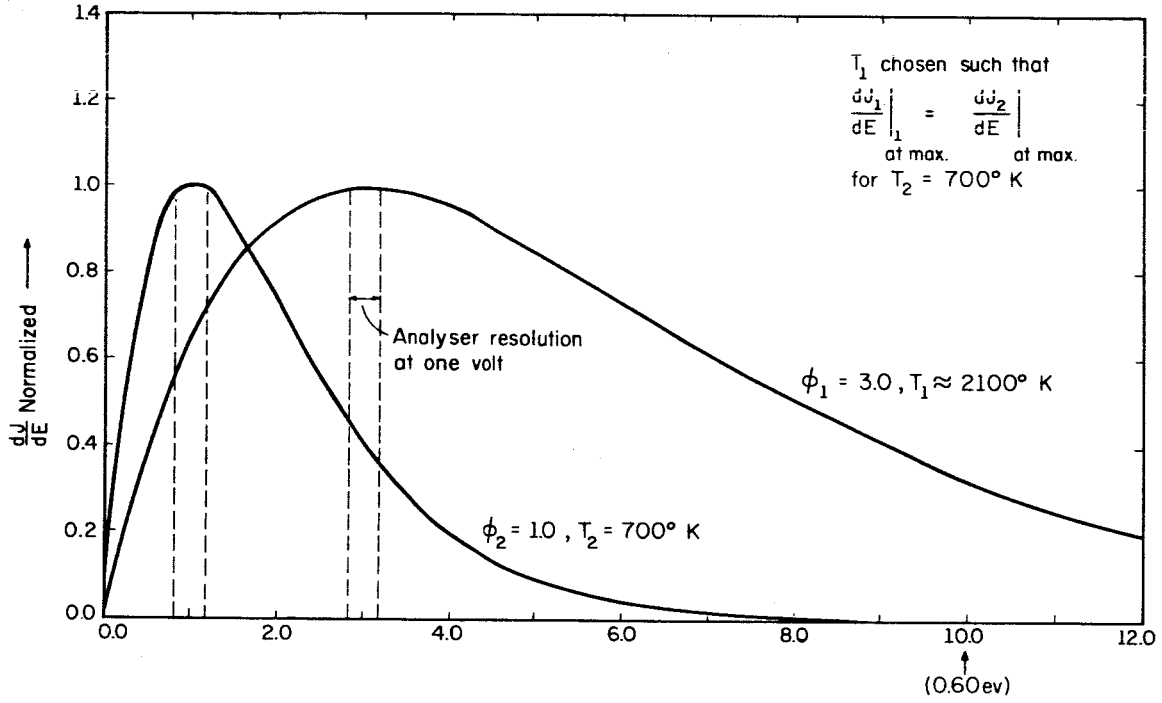

Fig. 3.4. Energy Distribution of Electron Thermally Emitted from Cathodes with Work Functions of 1.0 and 3.0 Volts.

cathode two. However, the effective current, that is the value at the maximum of the distribution, is the same in both cases. Since the monochromator accepts only a 20 mV slice of the total current, there is approximately K times as much unwanted current in the case of cathode two as for cathode one. Thus, the low temperature cathode is effective in reducing space charge.

As another effort to reduce space charge,[1] grids with collection plates behind them constitute several of the electrodes of the apparatus. The collection plates will attract spurious electrons which strike their surfaces, preventing the electrons from re-entering the beam region. The grid structures are incorporated at the output of the Pierce gun, as the deflecting plates in the monochromator and analyzer, and in the target chamber. The use of grids as the deflection plates in the monochromator is especially important, since space charge can be especially high in this region.

Fig. 3.5 illustrates why the grids should be spaced as closely as is reasonable. The potential curve is drawn assuming the two grids are at the same potential. The parabolic portion of the curve shows the variation of V across the space charge region. The sloped straight line portion is due to the E field which extends from the sheet of space charge to each of the grids. Since the E field depends only on the charge/area in the sheet, the slope remains the same as grid spacing changes. But the integral of the slope is the voltage and changes as

---

[1] Mermet, P. and Kerwin, L., Can. J. Phys., 38, 787 (1960).

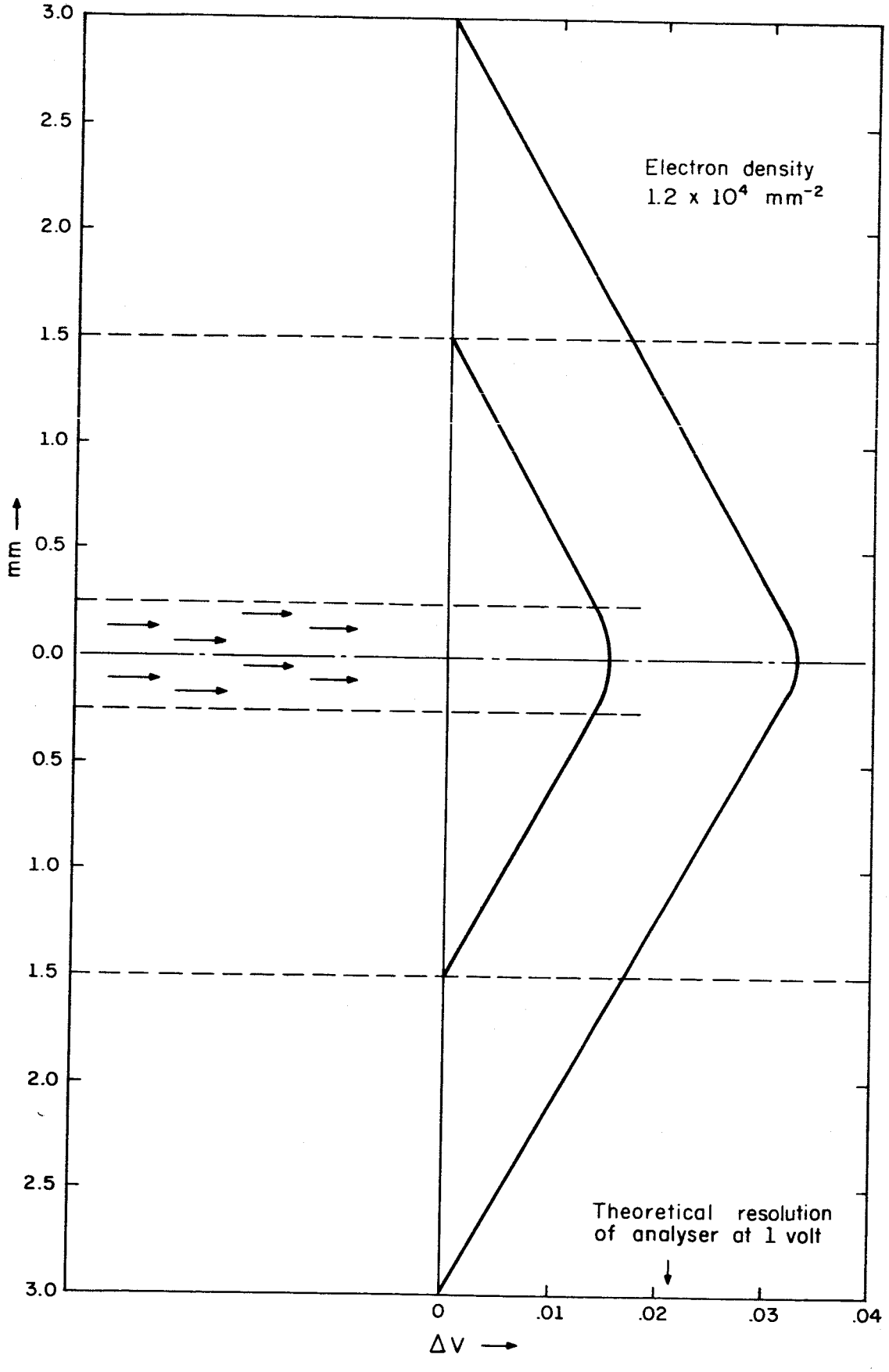

Fig. 3.5. Potential Produced by a Uniform Sheet of Space Charge.

the spacing changes. Thus, wider grid spacing allows the charge density of the beam to cause greater changes in the potential in the region of the beam. This effect causes electrons to have less kinetic energy than they would have without space-charge and can seriously affect the operation of the analyzer at low electron energies. (Note that the theoretical resolution of the analyzer at 1 volt is 0.02 volt which is the same magnitude as the space charge depression.)

3.2.3 Operation

There are several modes of operation of the apparatus. Fig. 3.6 shows voltage connections to the system. Some typical modes are:

1) With S_1 at a and $V_{SHIFT} = 0$, one can sweep $\mathcal{V}$ and obtain the energy distribution of electrons coming from the target for any primary energy chosen.

2) Doing the above with a positive value of V_{SHIFT} simply moves the distribution, obtained by procedure 1), over a distance V_{SHIFT} from zero.

3) With S_1 at a, $V_{SHIFT} = 0$, and $\mathcal{V}$ set to a given pass energy, one can obtain the variation of the height of a peak (say from an Auger process) at a given energy above the vacuum level of the target as a function of the primary energy.

4) With S_1 at b and $V_{SHIFT} = 0$, varying $\mathcal{V}$ allows one to continuously observe the height of a peak at some fixed voltage V_{Loss} below the primary energy as a function of the primary energy.

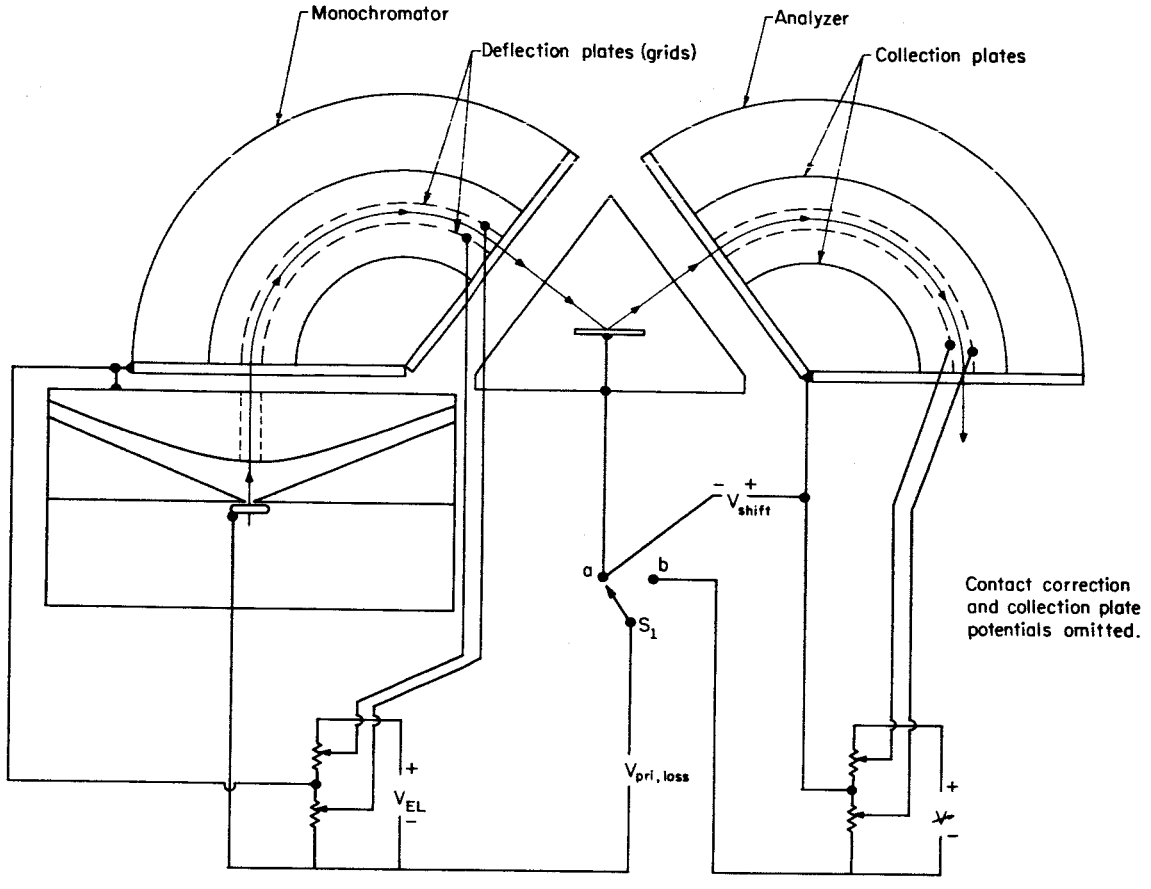

Fig. 3.6. Schematic of the Monochromator-Analyzer System, showing the electrical connections to the pertinent electrodes.

5) The energy distribution of 1) and 2) can be obtained without sweeping γ (and thus varying the analyzer resolution, which goes as 1/V). This is done by setting γ to some value and sweeping V_{SHIFT} to bring the electrons to the acceptance energy of the analyzer. This of course requires acceleration and deceleration between the target chamber and the second analyzer. A high transmission grid with wires transverse to the slit direction is placed across the exit of the target chamber. With this grid in place, the electric field is uniform where important and the electron trajectories can be calculated. A computer program was written to find the transfer ratio of electrons able to get from target into the second analyzer (with angle of entrance of less than $|\pm 3.5^{o}|$) for various acceleration and deceleration voltages. Fig. 3.7 shows these results with the transfer ratio normalized to one for zero acceleration.

3.2.4 Computer Control

This experiment operates under computer control. A schematic of the control system is shown in Fig. 3.8. The basic operation is very similar to a multichannel analyzer operated in the multiscaling mode. A digital-analog converter is stepped by the computer through 128 channels, a counter is operated for a preset time in each of the channels, and the number of counts is stored in temporary memory in the computer. This data can then be analyzed by the computer and displayed on a television monitor at the location of the experiment. The whole operation is controlled by a teletype keyset also located at the experiment. In addition to calling to the experiment programs written

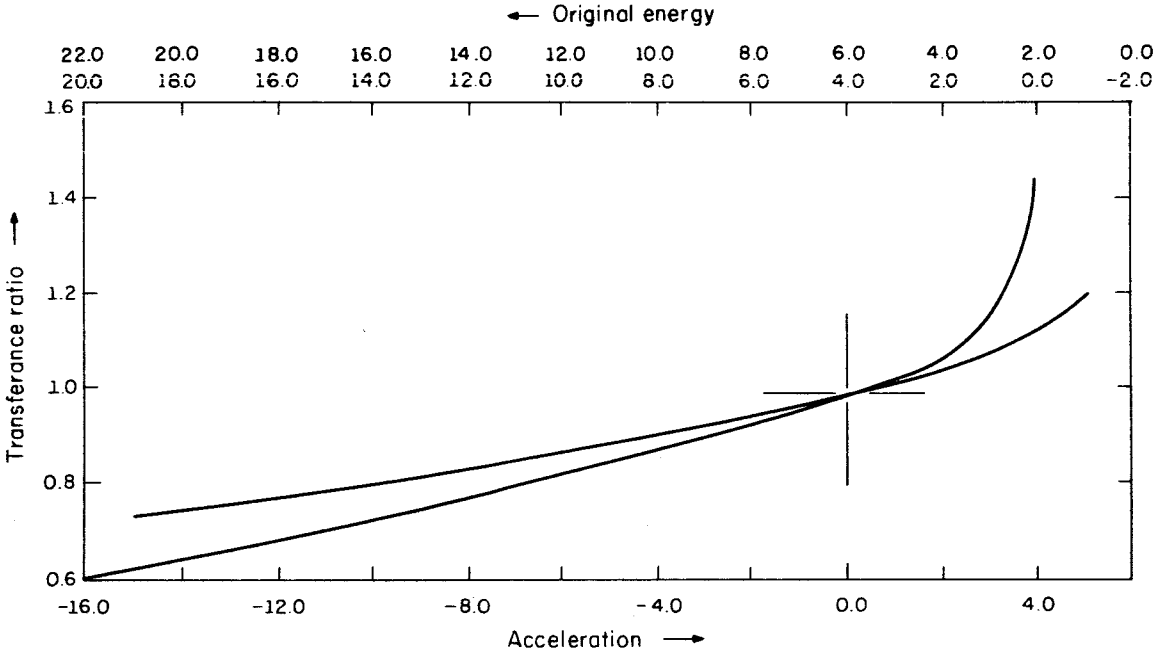

Fig. 3.7. Transfer Ratio of Current from Target Chamber to Analyzer as a Function of the Accelerating or Decelerating Voltage Applied between these Two Electrodes.

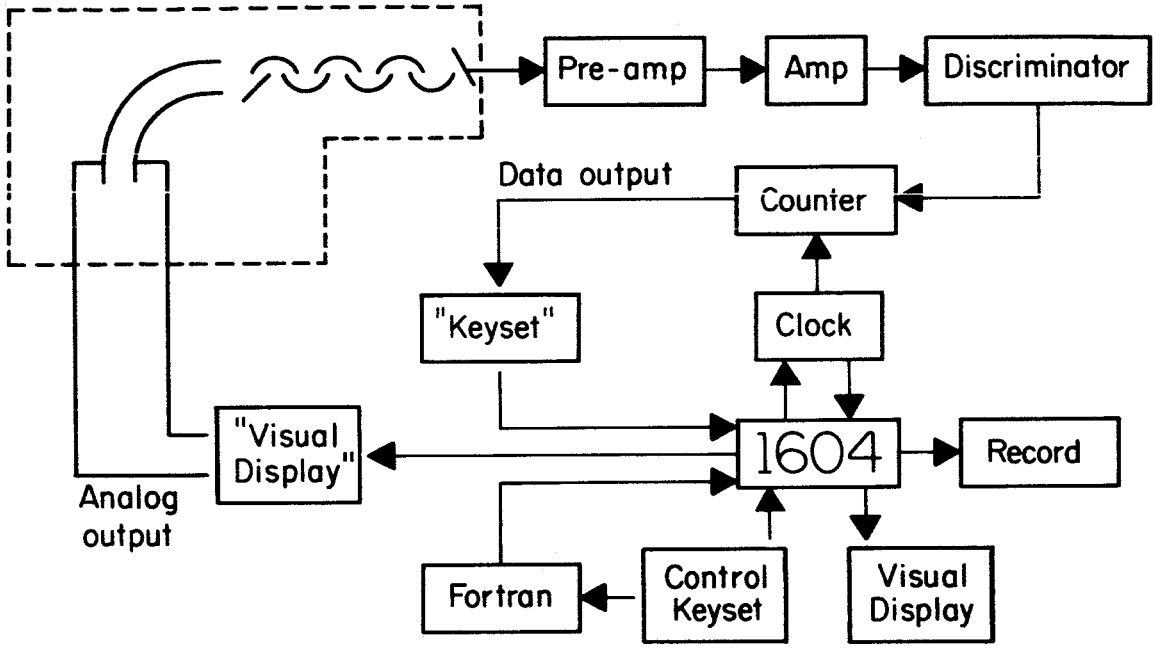

Block diagram of computer controlled secondary electron experiment

Fig. 3.8. Schematic of computer-controlled secondary electron experiment.

previously for the analysis of the data, Fortran statements can be written on the teletype keyset for performing analysis which was not anticipated. There are a number of significant aspects to this type of experimentation. These general aspects will be studied and constitute a substantial part of this portion of the program.

The computer-control part of this experiment is being done in cooperation with the PLATO teaching machine program of the Laboratory. The major portion of the buffer equipment is a part of that system. Programming and design of additional buffer equipment have been due also in large part to the PLATO group.

4. ANGULAR DISTRIBUTION OF AUGER ELECTRONS

Although the Auger neutralization effect[1] has been studied extensively during the last few years, a number of important questions still remain unanswered. Among these are:

(1) What is the angular distribution of ejected electrons?

(2) To what degree does the interaction between Auger and conduction band electrons influence the effect?

(3) To what degree does the crystal structure influence the effect?

(4) How does the effect depend on the angle of incidence of the ion beam?

An apparatus is being designed to perform three types of surface studies on a given crystalline surface in situ. The three measurements are:

(1) Auger neutralization

(2) Electron diffraction

(3) Secondary electron emission.[2]

It is hoped the correlation of these three types of measurements will provide definitive answers to the above questions. This study, in conjunction with the experiments described in the previous

---

[1] C.S.L. Technical Report, R-161.

[2] H. Bruining, Physics and Applications of Secondary Electron Emission, Pergamon Press, New York, 1954.

sections, should also provide a more coherent picture of surfaces and surface interactions.

The apparatus is shown schematically in Fig. 4.1. Low energy (<200 eV) ions or electrons impinge on a single crystal, tungsten target.[3] The scattered or ejected electrons pass through a slot in the shield and are collected by a collector of the Faraday cage or other design. Two grids attached to the collector make possible the direct measurement of the energy distribution of the ejected electrons. This is accomplished by modulating the ejected electron beam and using an A.C. detection technique similar to the one described in a previous report.[4]

The azimuthal angle, φ, is varied by rotating the target. The latitudinal angle, θ, is varied by rotating the collector. In the configuration shown in Fig. 4.1, interference between the ion gun and collector makes measurement of the distribution impossible for approximately 15^{o} of the latitudinal angle. If it is found that the angular distribution does not depend significantly on the angle of incidence of the ion beam, a second experimental configuration will be used. In this configuration the impinging ion or electron beam will be at an angle of about 15^{o} relative to a line normal to the target surface. With this arrangement, it will be possible to measure the ejected electron intensity over the entire 2π steradians.

---

[3] G. Tibbetts and F. M. Propst, R.S.J. 34, No. 11, 1268-1269.

[4] March, April, May 1963 Progress Report, p. 16.

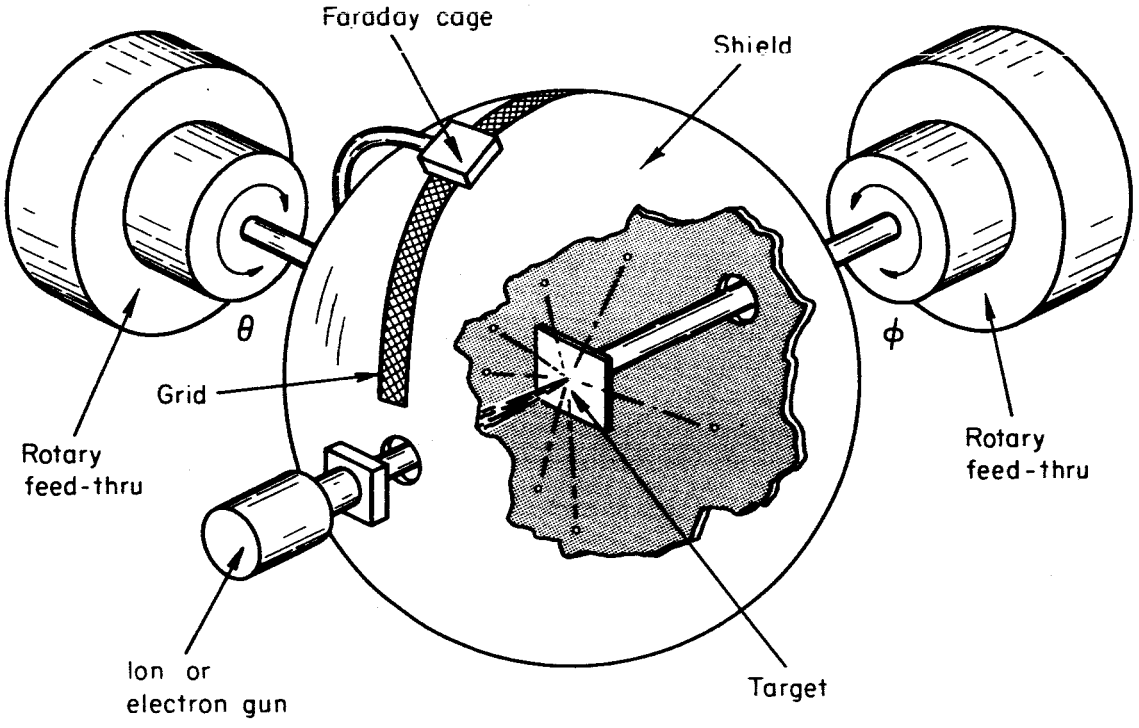

Fig. 4.1. Schematic of angular distribution experiment.

In order to rotate the Faraday cage and tungsten target, an ultrahigh vacuum rotary motion feedthrough, or vacuum crank, has been designed. Two such cranks are being constructed in the C.S.L. shop. A schematic of the crank is shown in Fig. 4.2.

The dotted line picture shows the position of the drive shaft and bushing assembly when the crank has been turned through 180^{o} relative to the solid line picture. The point A is fixed on the drive shaft and does not rotate relative to the vacuum system. The drive shaft is free to turn in the bushing assembly and drives the rotary output via a slot in the disk.

For bakeout the entire driving mechanism is slipped off by removing the bolts and holding the support posts to the bellows flange and by removing the nut on the drive shaft. A clamp has been designed to keep the bellows from collapsing due to atmospheric pressure. The crank should allow accurate positioning of counter and target, easy angular calibration, smooth rotary motion, and long bellows life.

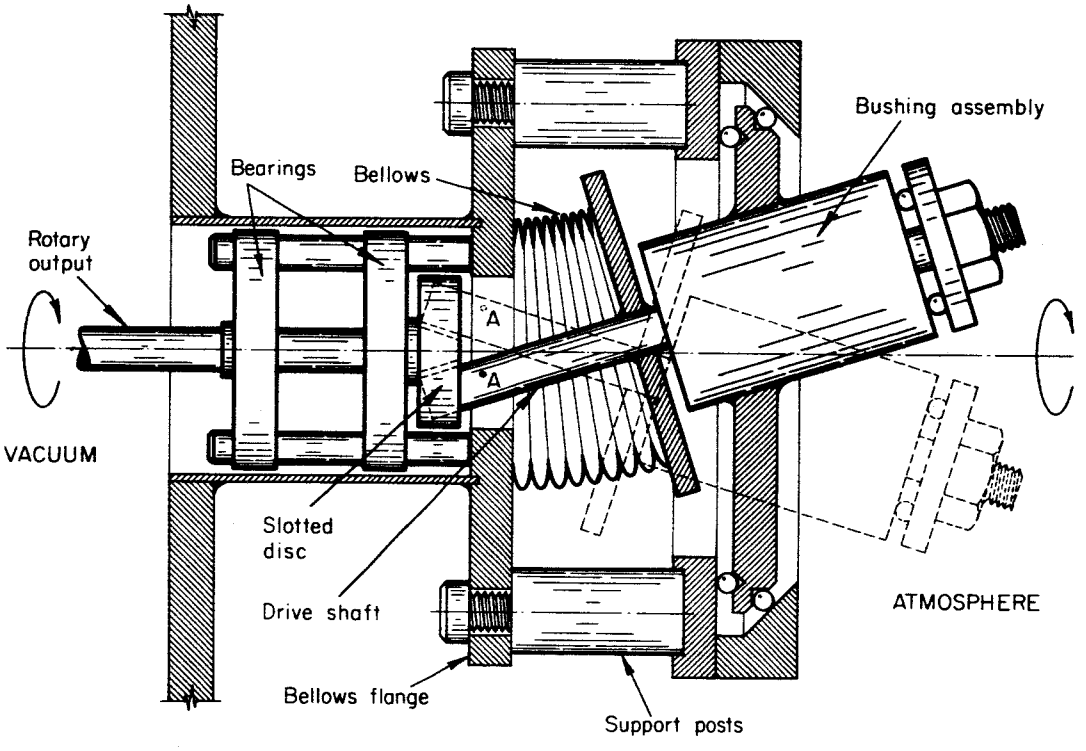

Fig. 4.2. Schematic of rotary motion feedthrough illustrating principle of operation.

5. STUDY OF THE ADSORPTION OF GASES ON METALS

Much of the work that has been done on the adsorption of gases on metallic surfaces has suffered from the inherent limitations of the standard methods. Coverage, θ, the fraction of possible adsorption sites which are filled by gas atoms, is the quantity whose measurement is most necessary.

When gas is adsorbed on the surface, there is a realignment of the electronic bonds on the surface metal atoms. The resulting change in work function, closely related to θ, may then be measured by many methods, all of which are rather difficult. Field emission studies have given direct, but difficult to reproduce, information about adsorbed surface atoms. Electron diffraction also has been successfully used; however, this technique fails when the scattering factor of the adsorbed species is much smaller than that of the substrate, or when the adsorbed gas replicates the crystallographic structure of the substrate.

One of the most commonly used techniques is the flashing of a metal filament to drive off the adsorbed gases and then measuring the consequent pressure rise within the system.[1] This method requires extreme precautions in relating the pressure rise to θ. Furthermore, as long, thin filaments are used, specific crystalline faces are not available. Since field-ion-microscope studies indicate that the

---

[1] Ehrlich, Journ. Chem. Ph. 34 No. 1, p. 29.

adsorption of gases has different characteristics on the different crystal faces, this method leaves many questions unanswered.

Migration of the gas atoms off the end of the filament when desorptive heating has begun can also decrease the amount of gas evolved, thus decreasing the value obtained for the desorption constant.

We intend to use the Auger process (emission of electrons by low energy incident ions) to measure the degree of surface coverage. In the clean surface case, He^+ ions incident on a metal interact with two electrons from the metal's conduction band. One of the electrons drops into the empty level, neutralizing the He^+ ion, and the other adsorbs the energy released in the process, ultimately being ejected from the metal in about ¼ of the cases. The ratio,

$$\gamma = \frac{\text{electrons ejected}}{\text{incident ions}}$$

is called the "Auger yield." Propst[2] has suggested that when gases are absorbed on the tungsten, the secondary electrons attempting to escape the metal are scattered back into the metal with a probability dependent on the coverage. Experimentally, θ is found to decrease almost linearly with increasing coverage until there is about one monolayer of adsorbed gas on the surface.

Thus, an observation of γ gives a direct and sensitive measure of θ, since the amount of high energy secondaries may decrease by a factor of 3 or more with adsorption of one monolayer of gas. Since

---

[2] Propst, F. M. and Lüscher, E., Phys. Rev. 132, No. 3., pp. 1037-1046, 1963.

only a small area of tungsten need be observed, it is possible to use single crystal material.

The apparatus shown in Fig. 5.1 is now under construction. Basically, we will use an electron impact Helium ion source, leading to a cylindrical lens which focuses the ions onto the target. The target is a single-crystal tungsten ribbon mounted on two heating leads which pass directly into a liquid nitrogen cooling bath. If the ion current is held constant by a feedback loop to the ion source, then γ is directly proportional to the current from the collector electrode.

The simple model of desorption process is analagous to the problem of a particle vibrating with a frequency ν in a potential well of depth E_B. An approximation to the escape probability will be,

$$\beta(T) = \nu e^{-E_B/kT} .$$

If there are several possible types of bonding wells available on the surface, as is suspected,

$$\beta(T) = \sum_i \nu_i e^{-E_{Bi}/kT} .$$

We will illustrate the experimental technique by considering desorption of a monatomic gas from the surface. First we flash the target clean and allow it to cool at time t_o (Fig. 5.2). At time t_1 the target has cooled, so that gas can be admitted, and the target exposed until the coverage increases to θ_o and the change in yield is $\Delta\gamma_o$. The gas flow is stopped at t_2. At time t_3 the target temperature is increased to temperature T_1 or T_2 so that thermal desorption begins.

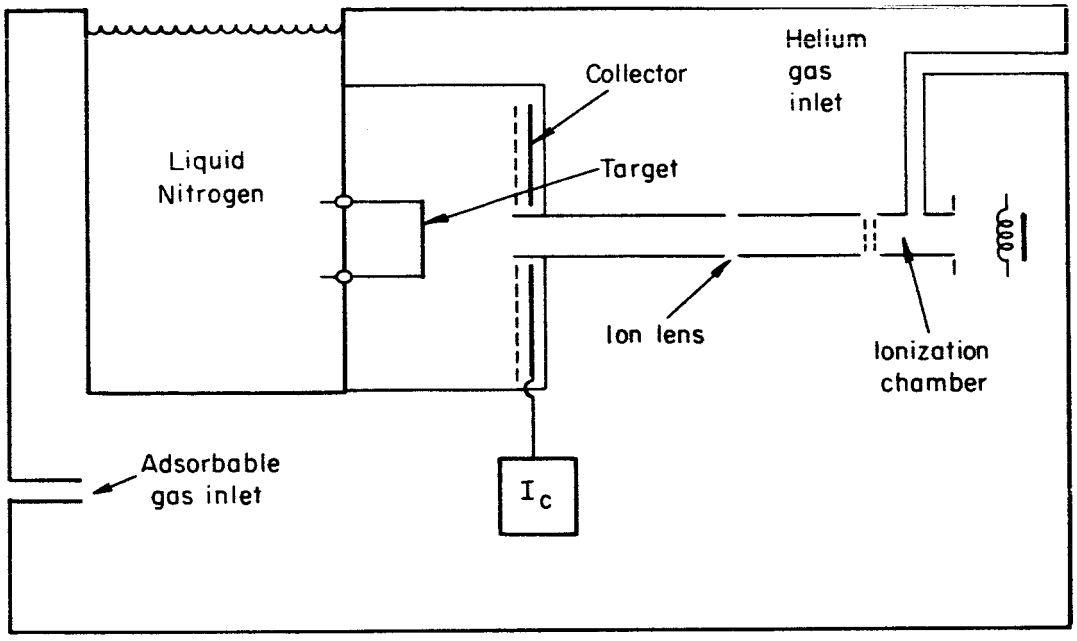

Fig. 5.1. Schematic of adsorption-desorption experiment.

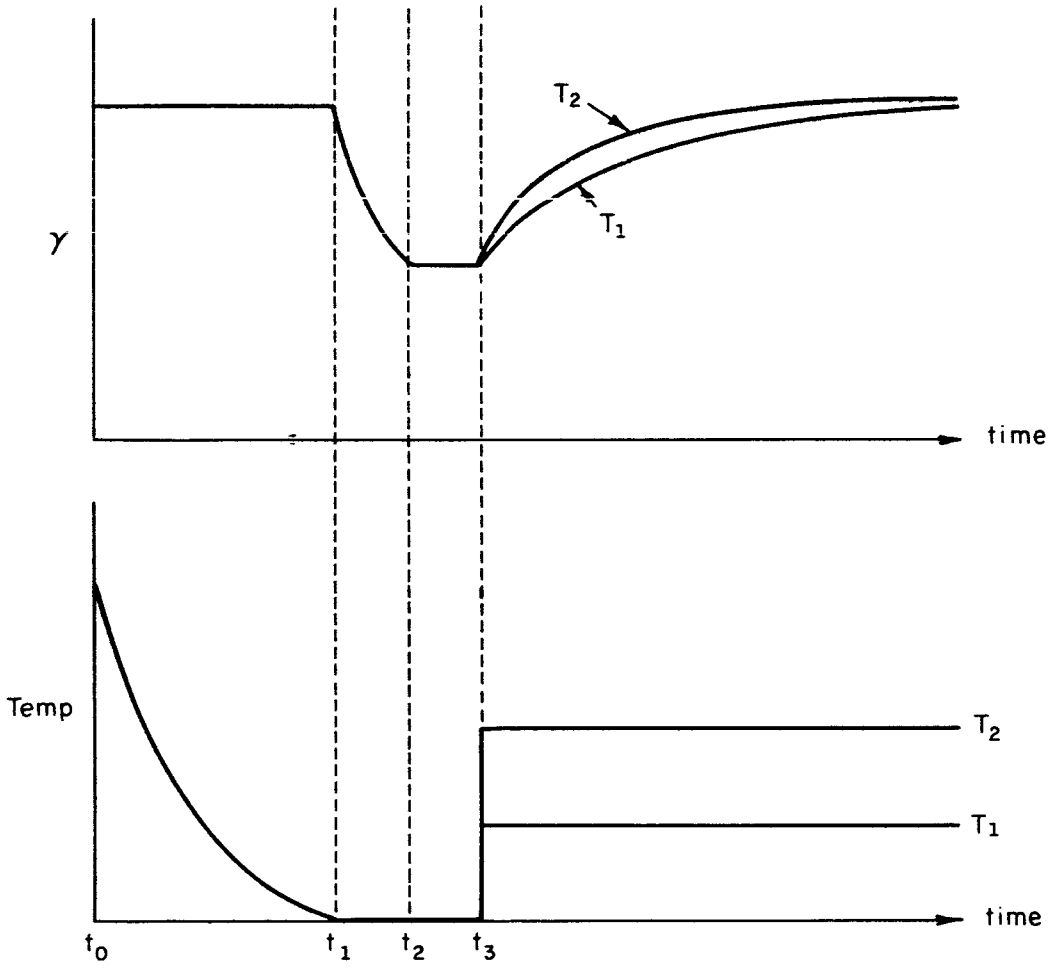

Fig. 5.2. Schematic illustrating the principle of one mode of procedure of the adsorption-desorption experiment.

As desorption continues, the values of the yield in both cases approach the clean surface value. We define the desorption coefficient $\beta(T)$ in this case by the equation,

$$\frac{d\theta}{dt} = -\beta(T)\,\theta$$

so that

$$\beta(T) = (1/t)\ln(\theta_o/\theta) = (1/t)\ln(\Delta\gamma_o/\Delta\gamma) \quad .$$

Thus by plotting $\ln(\Delta\gamma_o/\Delta\gamma)$ vs. t, we can find β from the slope. Non-linearities in the slope will reveal complexities in β, such as the small variation of β with θ.

This plotting procedure gives us one value of $\beta(T)$. By repeating the operation for a range of temperatures, T_1, T_2, ..., we will be able to construct the behavior of β with respect to T, and check with the simple model we have used to determine E_B and ν. We hope to be able to determine the number of bonding states and their energies from this information.

Finally, we note that this technique can be applied to various types of desorption, such as electron impact desorption, photodesorption, and ion sputtering.